RESEARCH ARTICLE

NANO · MICRO small
www.small-journal.com

Sulfur-Doped Carbon Dots as a Highly Selective and Sensitive Fluorescent Probe for Copper Ion Detection in Biological Systems

Minyoung Jin, Sanghee Lee, Su been Lim, Minyoung Lee, Jungwon Park, Hyun-Do Jung, Min-Ho Kang,* and Kun Na**

Copper ions are regarded as a double-edged sword since it plays a crucial role in biological functions but can also induce various severe diseases at imbalanced levels. However, conventional methods for quantifying copper ion (Cu^{2+}) levels often encounter complicated preparation procedures and interference from other substances. This study describes the one-pot microwave synthesis of sulfur-doped carbon dot (S_HICA) as a highly selective and sensitive fluorescent probe for Cu^{2+} detection in biological systems. S_HICA demonstrates improved fluorescence properties such as increased intensity and a red-shifted emission wavelength compared to carbon dots without sulfur (HICA), and S_HICA exhibits outstanding selectivity for Cu^{2+} through a fluorescence quenching effect. In vitro and ex vivo experiments are performed to validate the fluorescence selectivity of S_HICA, revealing that S_HICA has remarkable biocompatibility, fluorescence stability, and tolerance to varying pH levels. S_HICA presents significant potential as a fluorescent probe for detecting Cu^{2+} with elevated sensitivity and selectivity, as well as for the advancement of enhanced diagnostic tools that can monitor copper-related disorders in real time.

1. Introduction

Metal ions are crucial in various biological processes in plants and animals, as well as in humans. However, imbalances in the concentrations of metal ions within the human body might result in particular diseases. Thus, sensitive and selective techniques for the detection of metal ions are essential for the early diagnosis of illness, assessment of heavy metal poisoning, and personalized therapeutic approaches.[1–3] Many studies have focused on monitoring the concentrations of metal ions including potassium,[4] magnesium,[5] calcium,[6] iron,[7] and copper.[8] Specifically, abnormal levels of copper ions (Cu^{2+}) are directly associated with disorders such as Wilson's disease and Menkes syndrome, and they can also influence conditions such as Alzheimer's disease and Parkinson's disease.[9–11] The metabolism of copper is essential for several biological activities, including its function as a cofactor in enzymatic pathways related to antioxidant defense, DNA repair, cell division, and protein synthesis.[12–14] Serum copper levels are clinically significant for evaluating parameters associated with aging-related degenerative diseases, nutritional status, oxidative stress, inflammation, and immune abnormalities, all of which may influence carcinogenesis. Consequently, in vitro Cu^{2+} diagnostics utilizing blood or liquid-based biological samples have emerged as an essential tool for the accurate and early detection

M. Jin, S. been Lim, M.-H. Kang, K. Na
Department of BioMedical-Chemical Engineering
The Catholic University of Korea
Bucheon-si 14662, Republic of Korea
E-mail: mhkang@catholic.ac.kr; kna6997@catholic.ac.kr

M. Jin, S. been Lim, M.-H. Kang, K. Na
Department of Biotechnology
The Catholic University of Korea
Bucheon-si 14662, Republic of Korea

S. Lee
Department of Radiology
Feinberg School of Medicine
Northwestern University
Chicago, IL 60611, USA

M. Lee, J. Park
School of Chemical and Biological Engineering
Institute of Chemical Processes
Seoul National University
Seoul 08826, Republic of Korea

M. Lee, J. Park
Center for Nanoparticle Research
Institute of Basic Science (IBS)
Seoul 08826, Republic of Korea

H.-D. Jung
Division of Materials Science and Engineering
Hanyang University
Seoul 04763, Republic of Korea
E-mail: hdjung@hanyang.ac.kr

The ORCID identification number(s) for the author(s) of this article can be found under https://doi.org/10.1002/smll.202410765

DOI: 10.1002/smll.202410765

of copper-related diseases. Quantitative measurements of ion concentrations are crucial for diagnosing diseases, monitoring progression, predicting outcomes, and stratifying patients for targeted treatments.[15,16]

Conventional techniques for measuring Cu^{2+} levels have involved the complex preparation of biological samples (e.g., blood, urine, or liver tissue) followed by analysis using colorimetric methods, atomic absorption spectroscopy, and inductively coupled plasma mass spectrometry.[17] Colorimetric methods often encounter difficulties in measuring low concentrations accurately, and they may affected by interference from other biological substances.[18] Meanwhile, atomic absorption spectroscopy and inductively coupled plasma mass spectrometry require extensive sample preparation, expertise, and time. Therefore, efforts have been made to develop colorimetric sensors based on nanoparticles to simplify and enhance the detection process. Nanoparticle-based colorimetric sensors offer improved sensitivity for in vitro diagnostics because of the large surface area, enhanced binding and detection capabilities, and high selectivity, and the fast reaction time facilitates real-time measurements. They also have the potential for integration with other therapeutic tools. However, previously developed sensors such as organic dyes,[19] lanthanides,[20] and heavy metal quantum dots[21] suffer from issues including toxicity, low fluorescence stability, high costs, and insufficient sensitivity that have limited their applicability. Similarly, metal–organic frameworks (MOFs) also have been explored for Cu^{2+} detection,[22–24] but their poor water stability,[25] complex synthesis, and potential cytotoxicity[26] have limited their applicability in biological systems.

Despite these advancements, existing Cu^{2+} detection strategies still have limitations. Several techniques, including colorimetry, atomic absorption spectroscopy, and inductively coupled plasma mass spectrometry (ICP-MS) offer high Cu^{2+} detection sensitivity but often require extensive processing times and complex sample preparation. For instance, Muniz et al. reported an AE-based LC-ICP-MS method requiring 422 min per sample,[27] while Inagaki et al. utilized a 5 h pre-treatment process involving Chelex-100 resin.[28] Similarly, Lopez-Avila et al. demonstrated approach using an immunoaffinity chromatography followed by SEC-ICP-MS, involving a 30 min preparation and an additional 20 min separation process.[29] In addition, other Cu^{2+} detection methods such as colorimetric and fluorescence-based sensors frequently suffer from low detection limits and selectivity issues.

To overcome these challenges, carbon dots have emerged as a promising alternative because of their unique optical properties, high biocompatibility, cost-effectiveness, scalable synthesis, and versatility through surface functionalization.[30,31] These characteristics make carbon dots suitable for various applications including drug delivery,[32] energy materials,[33] bioimaging agents,[34] and sensors.[35] Carbon dots can be used as sensors by modifying their surface with functional groups to selectively interact with various chemical species including metal ions, organic molecules, and biomolecules. Various functional groups can be attached to facilitate the coordination and interaction with specific metal ions, which not only improves selectivity but also minimizes interference from other substances commonly found in biological environments.[36,37] Carbon dots can be modified with carboxyl, imidazole, and hydroxyl groups or doped with heteroatoms such as nitrogen and sulfur to enhance the selectivity and fluorescence intensity.[38,39] In particular, sulfur doping notably enhances the fluorescence stability and fluoresce intensity of carbon dots.[40–43] Moreover, the high surface-to-volume ratio of carbon dots provides abundant active sites for binding metal ions and greatly increasing the detection sensitivity.[44–46] Given these advantages, carbon dots are potentially superior to traditional nanoparticle-based sensors in terms of both sensitivity and selectivity particularly for metal ions present in trace amounts. Despite these advantages, most of the carbon dot-based sensors have been primarily focused on environmental applications rather than biological systems.[47,48] Additionally, most reported carbon dot-based Cu^{2+} sensors have been validated only at the in vitro level, limited applications in ex vivo or in vivo models.[49,50] For these reasons, we developed fluorescent sensor based on sulfur-doped carbon dots (S_HICA) for rapid, cost-effective, and highly sensitive for Cu^{2+} detection by fluorescence quenching. S_HICA has a response time of less than 5 min, which enables real-time monitoring, and does not require complex sample preparation or expensive instrumentation. The proposed method also exhibits competitive limit of detection (LOD) of 5.41 μM compared with conventional techniques such as other organic fluorescent probe, making it a promising candidate for practical applications, particularly in point-of-care diagnostics. S_HICA was prepared using a simple one-pot microwave synthesis method, and sulfur doping enhanced the fluorescence intensity compared with that of carbon dots without sulfur (HICA).[51,52] Comprehensive in vitro, in vivo and ex vivo experiments were performed to evaluate the Cu^{2+} detection performance of S-HICA under various conditions.

2. Results and Discussion

2.1. Synthesis and Physicochemical Properties

Figure 1 shows the synthetic procedure of S_HICA and its application to Cu^{2+} detection in biological systems. S_HICA is synthesized by reacting histidine and citric acid in dimethyl sulfoxide (DMSO) using microwave-assisted techniques (Figure 1a). For comparison, HICA was synthesized using the same precursors and method except that distilled water was used as the solvent. Citric acid and histidine act as sources of carboxyl and imidazole groups that enhance the ion detection capability and solubility of carbon dots. In addition, nitrogen doping from histidine and sulfur doping from DMSO enhances the fluorescence properties and ion detection sensitivity. These properties make S_HICA ideal for the selective detection of Cu^{2+} in biological systems (Figure 1b).

Figure 2 shows the characterization results for S-HICA. Dynamic laser scattering (DLS) was used to evaluate the size distributions of S_HICA (Figure 2a) and HICA (Figure S1, Supporting Information), which exhibited little variation with average particle sizes of 1.1 ± 0.3 and 1.2 ± 0.9 nm, respectively. Transmission electron microscopy (TEM) images of S_HICA (Figure 2b) and HICA (Figure S2, Supporting Information) was used to visualize the lattice fringes, which indicated a *d* spacing of 2.6 Å corresponding to the (100) spacing of graphite.[53] The X-ray

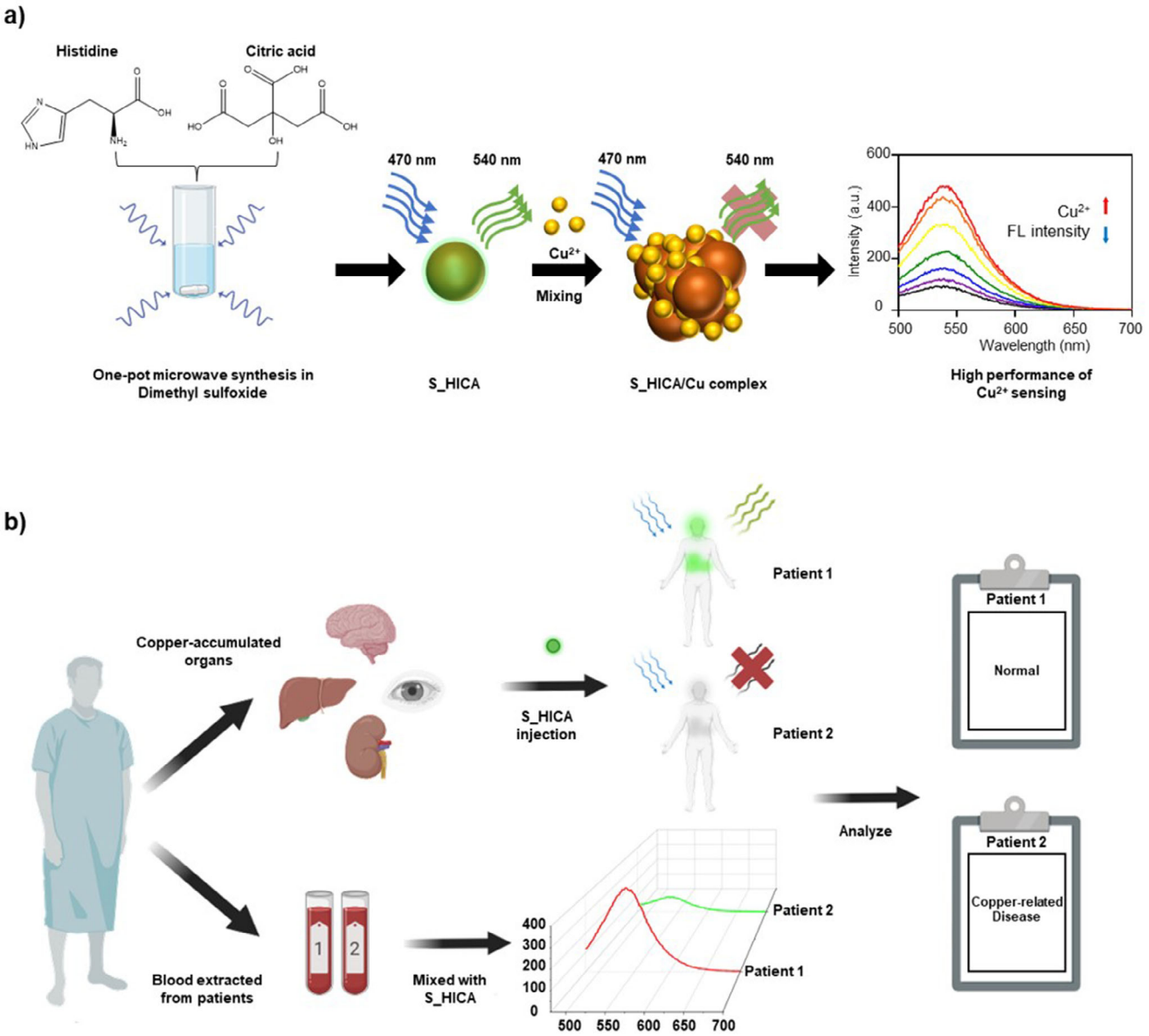

Figure 1. Synthesis and application of sulfur-doped carbon dot (S_HICA) to Cu^{2+} detection in biological systems. a) Synthetic procedure and fluorescence quenching mechanism. b) Application of S_HICA to diagnosing copper-related disorders. Graphical images were created with BioRender.com.

diffraction (XRD) patterns indicated that S_HICA (Figure 2c) and HICA (Figure S3, Supporting Information) had diffraction peaks with 2θ values of 21°–22°, which were attributed to the wide (002) spacing of carbon dots.[54] The UV–vis absorption spectra of S_HICA and HICA (Figure S4, Supporting Information) had two strong absorption bands at 200–220 nm ($\pi \rightarrow \pi^*$ transition) and 280–320 nm (n $\rightarrow \pi^*$ transition).[55] Atomic force microscopy (AFM) was used to investigate the morphology and size of S_HICA (Figure 2d–f), which had a particle height of ≈3.6 nm. X-ray photoelectron spectroscopy (XPS) was used to analyze the composition of S_HICA (Figure 2g), which exhibited five major peaks of O 1s, N 1s, C 1s, S 2s, and S 2p at 532, 400, 284, 227.6, and 162.6 eV, respectively. In contrast, HICA had only the three major peaks of O 1s, N 1s, and C 1s, but S 2s and S 2p were not detected (Figure S5, Supporting Information). Both S_HICA (Figure S6, Supporting Information) and HICA (Figure S5, Supporting Information) had the same binding energy peaks for the carbon, nitrogen, and oxygen spectra. However, only S_HICA exhibited obvious peaks at 162.7 eV ($S_{2p1/2}$) and 164.1 eV ($S_{2p3/2}$) (Figure 2h). Fourier transform infrared spectroscopy (FTIR) was used to analyze the chemical characteristics of S_HICA (Figure 2i) and HICA (Figure S7, Supporting Information), and the absorbance peaks for both were assigned to the stretching vibrations of O—H and N—H at 3375 cm^{-1},[56] —OH at 3179 cm^{-1},[57] and —C—H at 2924 cm^{-1}.[58] The peaks at 1700 cm^{-1} was attributed C═O stretching, commonly observed in carbon-based nanoparticles containing carboxyl functional groups.[59] The peak at 1437 cm^{-1} was attributed to C—N stretching.[60] The peak at 1599 cm^{-1}

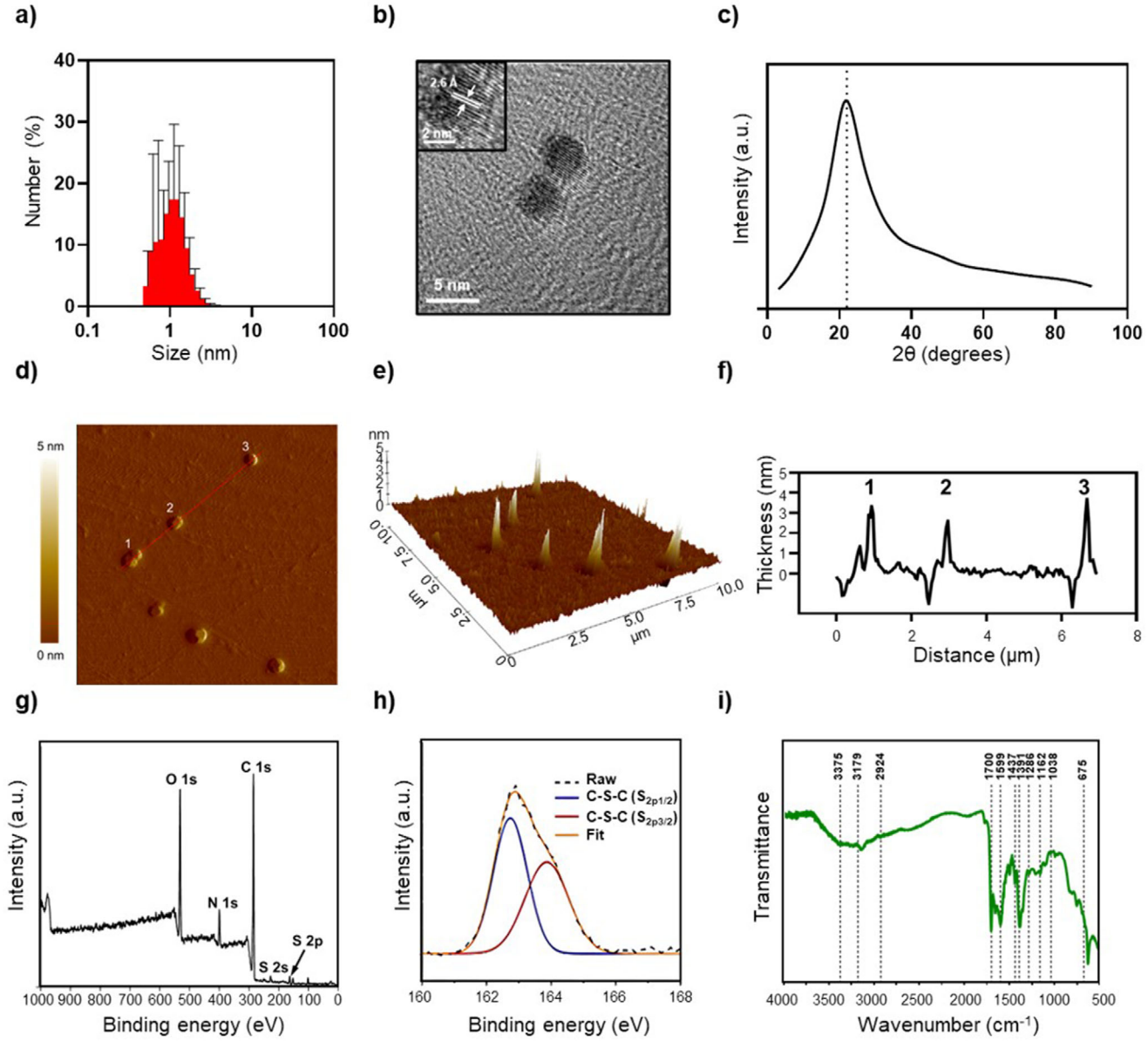

Figure 2. Characterization of S_HICA. a) Size distribution obtained by dynamic light scattering. b) Transmission electron microscopy image. c) X-ray diffraction spectrum. Atomic force microscopy results: d) amplitude, e) 3D image, and f) line profile of the red line in (d). g) Full X-ray photoelectron spectroscopy (XPS) spectrum and h) deconvoluted high-resolution XPS spectrum of S 2p. i) Fourier transform infrared spectrum.

corresponded to C—C stretching while the strong peak at 1391 cm^{-1} corresponded to C═C bond vibrations.[61,62] Absorption peaks at 1162 and 675 cm^{-1} were attributed to the flexural vibration of C—O and stretching vibration of C—H, respectively.[63,64] S_HICA also had peaks at 1038 and 1286 cm^{-1} corresponding to $-SO_3^-$ and C═S bonds that were absent in HICA.[65] Elemental analysis (Table S1, Supporting Information) showed that S_HICA had an atomic composition of 17.03% N, 48.54% C, 5.21% H, 22.08% O, and 7.24% S while HICA had an atomic composition of 18.59% N, 40.48% C, 6.21% H, and 34.49% O. These results confirm that the carbon dots were successfully doped with sulfur in S_HICA. Overall, S_HICA and HICA had similar physicochemical properties in terms of size, degree of crystallization, and elemental composition, which suggests that HICA can serve as a control in further studies.

2.2. Fluorescence Properties

Figure 3 compares the optical properties of S_HICA and HICA. Carbon dots fluoresce owing to their unique structure and surface chemistry.[66,67] The excitation (Ex)–emission (EM) intensity spectra of HICA (Figure 3a) and S_HICA (Figure 3b) reveal a significant redshift in the fluorescence emissions upon sulfur doping. The maximum fluorescence intensity of HICA was observed at 340/415 nm, while that of S_HICA shifted to

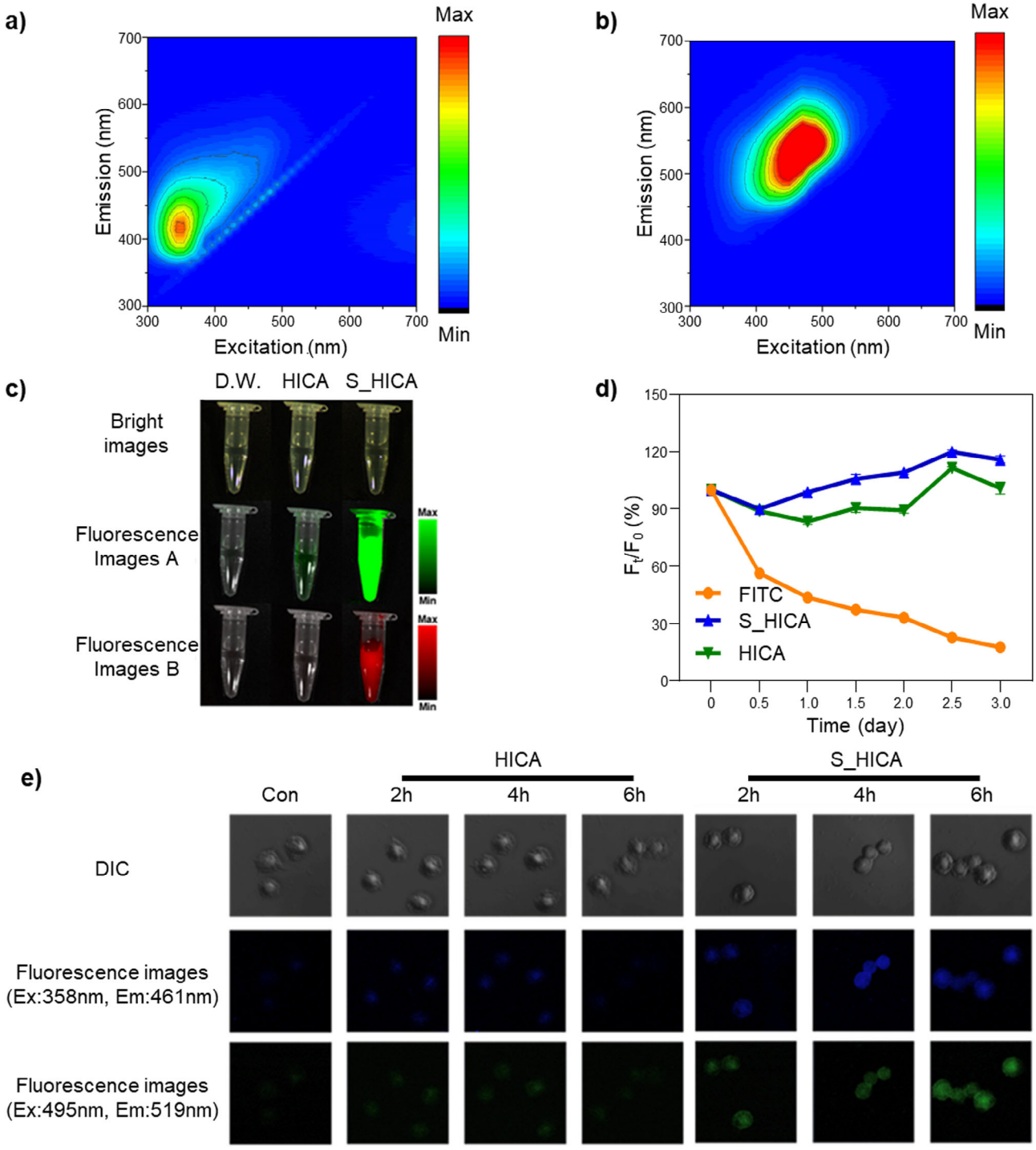

Figure 3. Fluorescence properties of S_HICA. Excitation–emission intensity spectra of a) HICA and b) S_HICA. c) Fluorescence images of HICA and S_HICA. (Fluorescence image A: Ex: 470nm, Em: 530 nm and fluorescence image B: Ex: 530nm, Em:630nm) d) Fluorescence stability assay depending on time (n = 3). e) Confocal differential interference contrast (DIC) and fluorescence images of L929 cells incubated with HICA and S_HICA.

470/535 nm. This redshifted fluorescence emission spectrum suggests that sulfur doping modifies the electronic structure of carbon dots, enhancing their fluorescence properties at longer wavelengths. Fluorescence images of S_HICA and HICA at a concentration of 1 mg mL^{-1} in distilled water (Figure 3c) indicated that both carbon dots exhibited fluorescence in two distinct channels: one with an Ex wavelength of 470 nm and Em wavelength of 530 nm, and the other with an Ex wavelength of 530 nm and Em wavelength of 630 nm. Notably, S_HICA exhibited a superior fluorescence intensity in both channels

compared to HICA. Moreover, HICA exhibited minimal fluorescence at longer wavelengths, which underscores its limited utility in broader applications. Doping carbon dots with heteroatoms such as nitrogen, sulfur, or phosphorus can modify their electronic properties and enhance fluorescence.[68–70] These results show that S_HICA had a greater fluorescence intensity and redshift in the emission wavelengths compared with HICA, which indicates its potential as an advanced and highly efficient fluorescent probe.

For in vitro diagnostics using biological samples, the fluorescence of a probe needs to be stable under diverse environmental conditions to ensure accurate and reliable results. Biological samples may contain various enzymes with acids or bases that can destabilize or change fluorescent materials. The fluorescence intensity of S_HICA was monitored at various time points (Figure 3d) and at different pH conditions (Figures S8 and S9, Supporting Information). Fluorescein-5-isothiocyanate (FITC) is a widely used fluorescence agent and was used here as the positive control. S_HICA demonstrated superior fluorescence stability compared with FITC by maintaining the fluorescence intensity over an extended period while the fluorescence intensity of FITC rapidly diminished within a few hours. S_HICA also showed consistent performance across a range of pH conditions whereas FITC experienced a substantial loss of fluorescence intensity in both acidic and alkaline environments. To further investigate the stability of S_HICA, we evaluated the fluorescence response of S_HICA at various temperatures ranging from 20 to 80 °C. The results revealed that S_HICA retained fluorescence intensity even at high temperatures (80 °C), confirming the robust thermal stability of S_HICA (Figure S10, Supporting Information). These results highlight the promise of S_HICA as a fluorescent probe for biological applications owing to its exceptional fluorescence stability and pH tolerance and thermal stability. The fluorescence stability of S_HICA not only facilitates long-term analysis but also enhances its detection capabilities at low concentrations by reducing the risk of false positives caused by signal degradation and improving the measurement reproducibility and accuracy.

To evaluate the applicability of S_HICA to detecting Cu^{2+} in biological systems, the cytotoxicity was assessed by using the 3-(4,5-dimethylthiazol-2-yl)-2,5-diphenyltetrazolium bromide (MTT) assay (Figure S11, Supporting Information). The results indicated that S_HICA had high biocompatibility at concentrations of 0–10 mg mL^{-1}. Flow cytometry revealed that the fluorescence intensity of L929 cells incubated with S_HICA exhibited strong correlations with both time and concentration (Figure S12, Supporting Information). Images of L929 cell pellets confirmed the cellular uptake of both S_HICA and HICA (Figure S13, Supporting Information). Notably, L929 cell pellets treated with S_HICA emitted a stronger fluorescence intensity in both channels (Ex/Em: 470 nm/530 nm and 530 nm/630 nm) compared to those treated with HICA. Next, L929 cells were treated with S_HICA and HICA, and confocal microscopy was used to evaluate the suitability of S_HICA as a fluorescent dye for cell imaging (Figure 3e). For both carbon dots, the fluorescence intensity gradually increased over time in both channels (Ex/Em: 358 nm/461 nm and 495 nm/510 nm). Cells exposed to S_HICA exhibited a noticeably higher fluorescence intensity than cells exposed to HICA. These results indicate that carbon dots can accumulate within cells, which suggests that they can be used to detect ions in the surrounding medium as well as intracellular systems. Notably, S_HICA provided a comparable fluorescence intensity as HICA at a lower concentration. Its superior sensitivity allows the amount used to be minimized, which can reduce the associated toxicity.

Figure 4 shows the Cu^{2+} detection selectivity of S_HICA. A screening process was performed using various metal ions (i.e., Fe^{3+}, Gd^{3+}, Al^{3+}, Mg^{2+}, Cu^{2+}, Cd^{2+}, K^{+}, and Cs^{+}) with the chloride ion (Cl^{-}) at concentrations of 0–500 μM (Figure 4a). The analysis was conducted with S_HICA solutions at a concentration of 0.1 mg mL^{-1} in distilled water. S_HICA only exhibited a concentration-dependent fluorescence quenching effect when mixed with Cu^{2+}. Such a quenching effect was not observed with the other metal ions. The correlation between the fluorescence intensity of S_HICA and the Cu^{2+} concentration was assessed across various Ex and Em wavelengths (Figure 4b,c; Figure S14, Supporting Information). The fluorescence intensity decreased gradually as the Cu^{2+} concentration increased from 0 to 1000 μM. In particular, the ratio between the current and initial fluorescence intensities (I/I_0) had a high correlation coefficient ($R^2 = 0.97$) with Cu^{2+} concentrations of 0.98–125 μM. To validate the sensitivity of our S_HICA-based Cu^{2+} detection platform, we compared its LOD with that of previously reported fluorescent sensors. S_HICA exhibited an LOD of 5.41 μM, demonstrating competitive sensitivity compared to other sensors. For instance, a functionalized oligomeric fluorescent sensor exhibited LOD of 10.4 and 9.88 μM,[71] while a water-soluble organic fluorescent probe showed an LOD of 9.68 μM.[72] Similarly, a photochromic dendrimer-based probe demonstrated a LOD of 10 μM.[73] These results indicate that S_HICA has a superior detection capability, making it a promising candidate for Cu^{2+} monitoring in biological applications. In addition, fluorescence images of S_HICA solutions mixed with various concentrations of Cu^{2+} showed a gradual decrease in fluorescence intensity as the Cu^{2+} concentration increased (Figure S15, Supporting Information). These results demonstrate the potential of S_HICA as a Cu^{2+} sensor owing to its high selectivity and sensitivity, even at minimal concentrations.

Figure 5 shows the quenching mechanism of S_HICA in the presence of Cu^{2+}. S_HICA and Cu^{2+} were mixed and maintained at room temperature for 30 min, followed by heating to 80 °C for 10 min, and cryo-TEM images were obtained for S_HICA, mixed S_HICA and Cu^{2+}, and mixed and heated S_HICA and Cu^{2+} samples (Figure 5a). Adding Cu^{2+} to S_HICA formed a S_HICA/Cu^{2+} complex that was not observed in pure S_HICA, and the amount of the complex increased with the increase of Cu^{2+} concentration leading to formation of visible aggregation (Figure S16, Supporting Information). To confirm the chemical structural properties of the S_HICA/Cu^{2+} complex, we conducted Selected Area Electron Diffraction (SAED) analysis (Figure S17, Supporting Information). The SAED pattern indicated that the complex has amorphous structure, contrast to CuS or other crystalline nanoparticles.[74] In order to further investigate the quenching mechanism of S_HICA, the fluorescence lifetime of S_HICA (Figure 5b) were measured at different Cu^{2+} concentrations. The fluorescence lifetime of S_HICA showed two distinct components. The long component is attributed to the core of the S_HICA, while the shorter component originates

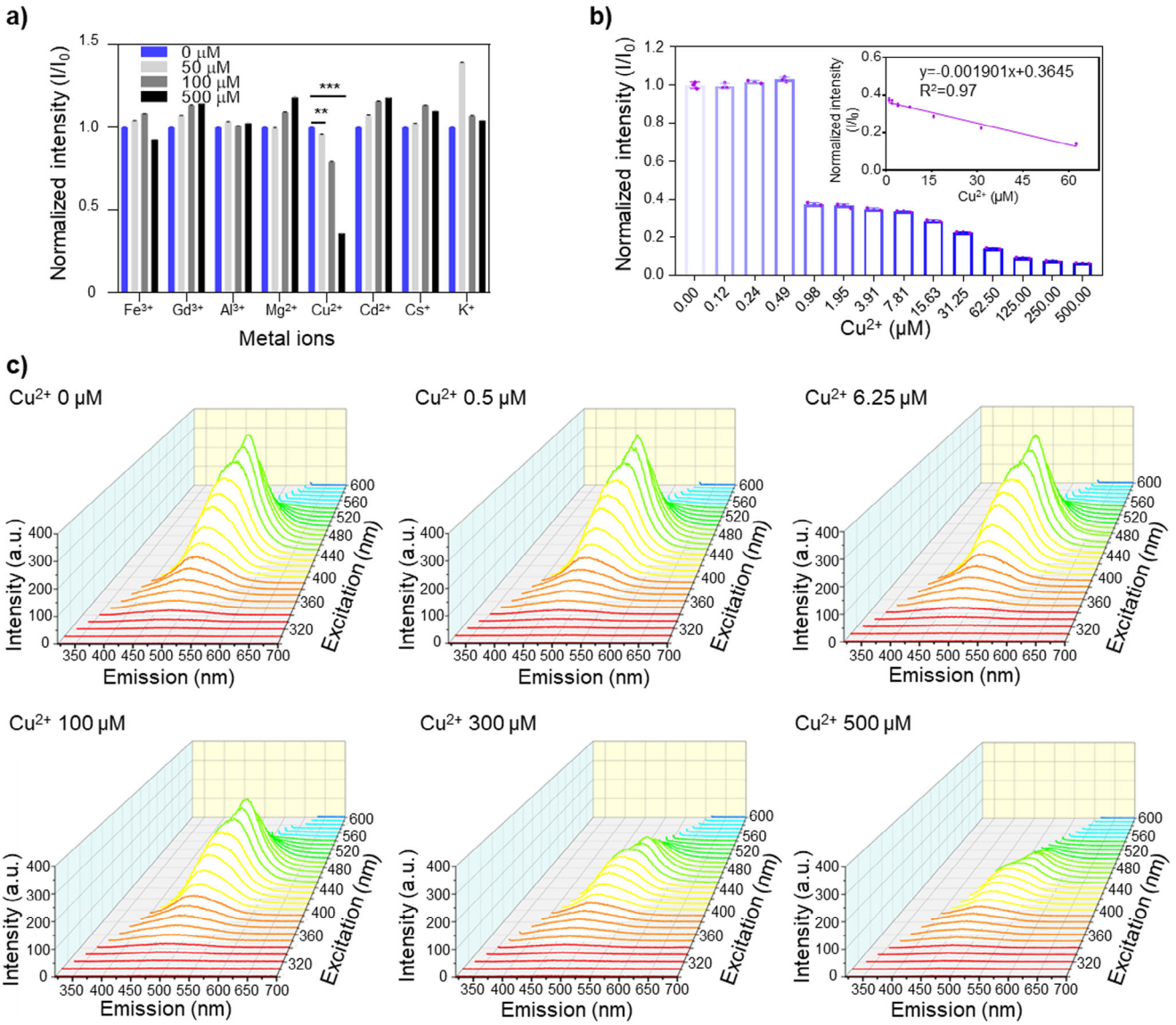

Figure 4. Detection of Cu^{2+} using S_HICA. a) Relative Fluorescent intensity of S_HICA in the presence of various metal ions (n = 3). b) Relative fluorescent intensity (inset: linear relationship between I/I_0 of S_HICAs and the concentration of Cu^{2+}, n = 3) and c) fluorescent spectra of S_HICA (0.1 mg mL^{-1}) with Cu^{2+} at different concentrations. (***$p < 0.001$, Two-way Anova with Turkey)

from the surface group of S_HICA.[75] Despite the addition of Cu^{2+}, the fluorescence lifetime exhibited negligible changes, further supporting that the quenching mechanism follows a static quenching pathway. Temperature dependent fluorescence intensity measurements of S_HICA/Cu^{2+} complex (Figure 5c) confirmed that the fluorescence intensity gradually increased upon heating. This result indicates that fluorescence quenching occurs due to the formation of the S_HICA/Cu^{2+} complex. As the temperature increased, the complex dissociated, leading to the fluorescence recovery. The result is consistent with the Cryo-TEM images, which also showed the dissociation of S_HICA/Cu^{2+} complex upon heating. Additionally, upon heating, the size of the complex decreased. UV–vis absorbance analysis (Figure 5d) revealed a new absorbance peak at 810 nm as the temperature increased for the S_HICA/Cu^{2+} complex sample. To further verify that fluorescence quenching occurs via complex formation between S_HICA and Cu^{2+}, we performed fluorescence measurements using FOBI. Since Ethylenediaminetetraacetic acid (EDTA) is well known as a metal chelator, we hypothesized that it would effectively prevent S_HICA/Cu^{2+} complex formation and fluorescence quenching. To test this, we prepared three groups including S_HCIA alone, S_HICA with a pure Cu^{2+} solution, or with a pre-mixed Cu^{2+}/EDTA solution. The results showed significant fluorescence quenching in the presence of Cu^{2+}. However, in the presence of the pre-mixed Cu^{2+}/EDTA solution, fluorescence quenching was significantly reduced (Figure S18, Supporting Information). These results suggest that the S_HICA/Cu^{2+} complex forms by the adsorption of Cu^{2+} onto S_HICA. Increasing the temperature destabilizes the complex and leads to the desorption of Cu^{2+}, which indicates a static

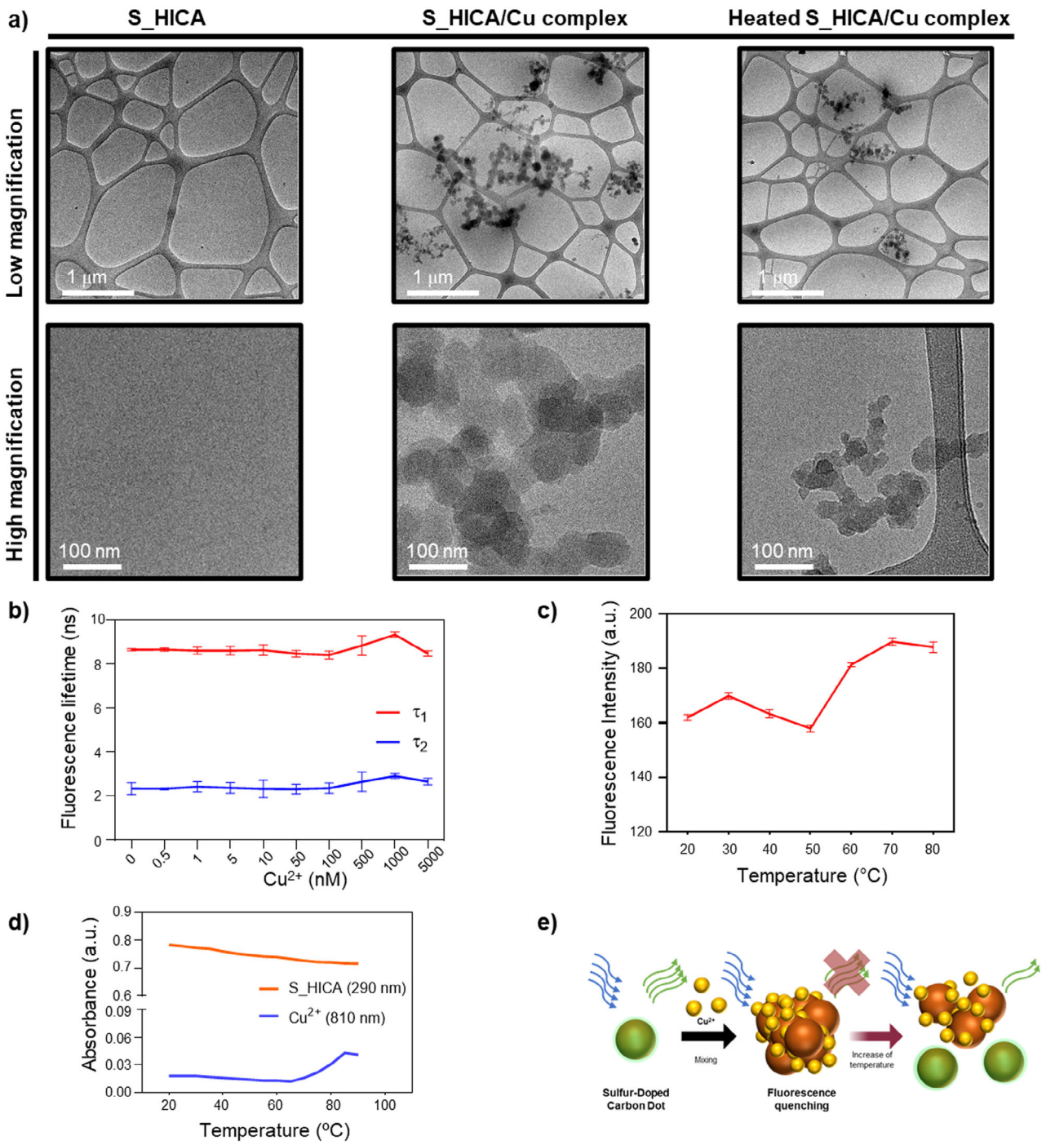

Figure 5. Quenching mechanism of S_HICA in the presence of Cu^{2+}. a) Cryo-TEM images of S_HICA, S_HICA/Cu^{2+} complex and S_HICA/Cu^{2+} complex when heated to 80 °C. b) Fluorescence lifetime of S_HICA under the various Cu^{2+} concentrations (n = 3). c) Fluorescence intensity of S_HICA/Cu^{2+} complex at different temperatures (n = 3). d) UV–vis absorbance spectra of S_HICA and Cu^{2+} in S_HICA/Cu^{2+} complex at different temperatures. e) Fluorescence quenching for Cu^{2+} detection and dissociation by heating. Graphical images were created with BioRender.com.

quenching mechanism for S_HICA (Figure 5e).[76] These results collectively indicate that S_HICA/Cu^{2+} complex formation is responsible for fluorescence quenching. Under the increased temperature, the complex destabilizes, allowing fluorescence recovery.

2.3. Application to Biological Systems

Figure 6 shows the results of in vitro and ex vivo experiments that were conducted to evaluate the potential clinical applications of S_HICA, particularly as a probe for copper-related diseases.

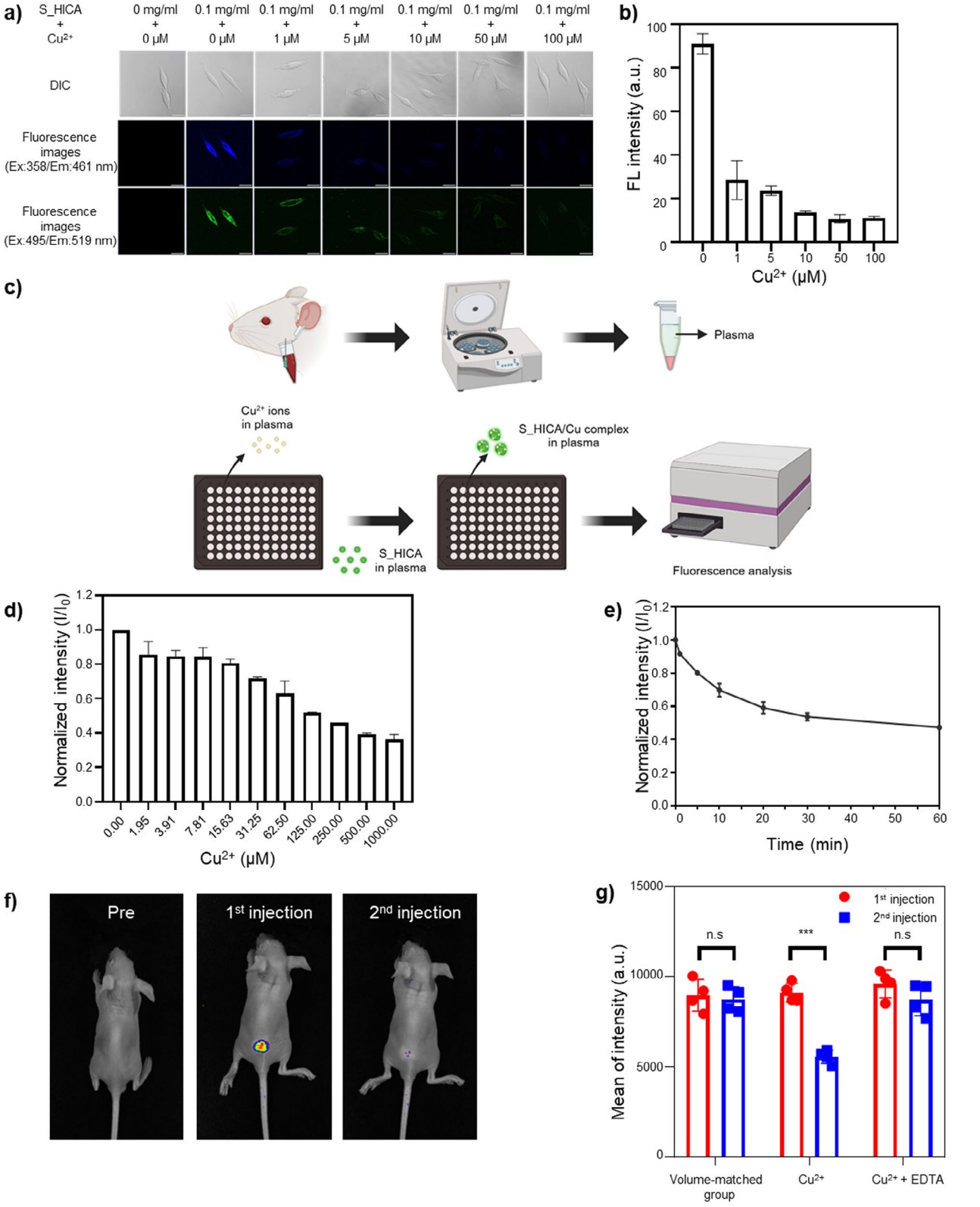

Figure 6. Application of S_HICA to detect Cu^{2+} in biological systems in vitro, ex vivo and in vivo. a) Confocal microscopy images of L929 cells treated with various concentrations of Cu^{2+} (0–100 μM) followed by 0.1 mg mL^{-1} of S_HICA. b) Fluorescence intensity of S_HICA at an excitation wavelength of 495 nm and emission wavelength of 519 nm. c) Schematic of the ex vivo experiment. Fluorescence response of S_HICA to the d) Cu^{2+} concentration and e) incubation time in ex vivo. f) Fluorescence images of mice injected with S_HICA before and after the administration of Cu^{2+}. g) Quantitative analysis of fluorescence intensity at the injection site (n = 4) (***$p < 0.001$, n.s, not significant, Two-way ANOVA with Sidak's multiple comparisons test).

L929 cells treated with Cu^{2+} showed no observable toxicity up to a Cu^{2+} concentration of 100 µM, which established this value as the maximum concentration for subsequent experiments (Figure S19, Supporting Information). To assess the fluorescence performance of S_HICA in the presence of Cu^{2+}, L929 cells were pre-incubated with varying Cu^{2+} concentrations (0–100 µM) for 4 h followed by treatment with 0.1 mg mL^{-1} of S_HICA. Confocal microscopy confirmed that the fluorescence intensity of S_HICA within the L929 cells decreased as the Cu^{2+} concentration increased (Figure 6a), which provides evidence that S_HICA can effectively sense the Cu^{2+} concentration in a cellular environment. The fluorescence intensity of S_HICA was quantified by using the software ImageJ (Figure 6b), and the results indicated that the fluorescence intensity decreased noticeably with a minimal Cu^{2+} concentration of 1 µM and that it had an inversely proportional relationship with the Cu^{2+} concentration. These results suggest that patients with copper-related diseases such as Alzheimer's, Parkinsons's and Wilson's diseases can be injected with S_HICA to monitor Cu^{2+} levels in the body by fluorescence imaging.

For the ex vivo experiments, blood samples were collected from the cheeks of mice, and the serum was subsequently isolated after which varying concentrations of Cu^{2+} and S_HICA (0.1 mg mL^{-1}) were mixed in the serum (Figure 6c). The fluorescence intensity of S_HICA was measured in relation to the Cu^{2+} concentration (Figure 6d) and incubation time (Figure 6e). The fluorescence intensity noticeably decreased as the Cu^{2+} concentration increased within a few minutes. To investigate the applicability of S_HICA for in vivo detection, we conducted fluorescence imaging experiments in live mice via subcutaneous injection following protocols described in previous studies.[77,78] First, 50 µL of S_HICA was first injected on the back of the mice. Following the initial injection, fluorescence imaging was performed using FOBI, which confirmed the strong fluorescence at the injection site. To evaluate the fluorescence response to Cu^{2+}, mice were divided into three groups: 1) S_HICA group, where an equal volume of dilution solution was injected to match the total volume to other groups, 2) a pure Cu^{2+} (50 µL, 200 µM) solution group and 3) a pre-mixed Cu^{2+}/EDTA (50 µL, 200 µM) solution group, with each solution injected at the S_HICA injected site. The fluorescence intensity of S_HICA significantly decreased in the presence of Cu^{2+}, whereas in the dilution solution group and Cu^{2+}/EDTA group, the fluorescence intensity of S_HICA remained relatively unchanged (Figure 6f,g; Figure S20, Supporting Information). These results strongly support the potential of S_HICA for Cu^{2+} detection in biological environments and confirm that the fluorescence quenching mechanism is associated with S_HICA/Cu^{2+} complex formation, supporting static quenching. Overall, the ability of S_HICA to selectively detect Cu^{2+} through fluoresce quenching across in vitro, ex vivo, and in vivo conditions highlights the potential of S_HICA for real-time Cu^{2+} level monitoring in biological systems.

3. Conclusion

S_HICA was successfully synthesized through a facile one-pot microwave-assisted method. S_HICA exhibited excellent fluorescence properties with enhanced intensity and red-shifted wavelengths compared to HICA. Sulfur doping not only improved fluorescence efficiency but also enabled longer-wavelength excitation, which enhanced tissue penetration and reduced autofluorescence interference. In addition, S_HICA demonstrated high Cu^{2+} selectivity through a fluorescence quenching effect that was absent for other metal ions. To further evaluate the sensing capability of S_HICA, sensing parameters including the limit of detection (LOD), detection range, sensitivity, stability and response time were analyzed. The detailed analysis results of this analysis are summarized in Table S2 (Supporting Information). The in vitro and ex vivo experiments confirmed that the fluorescence intensity of S_HICA noticeably decreased upon exposure to Cu^{2+}. The results indicate that S_HICA can potentially be applied to diagnosing copper-related diseases such as Alzheimer's, Parkinsons's, and Wilson's diseases. In addition, the fast response time indicates that S_HICA can be used for real-time monitoring of Cu^{2+} levels as an efficient and reliable diagnostic tool. S_HICA represents a significant advance in the biosensing field as an effective fluorescent probe for detecting and monitoring Cu^{2+} levels in biological systems that will ultimately contribute to improved healthcare outcomes and environmental safety. S_HICA addresses the drawbacks of conventional metal ion sensors and holds much promise for timely diagnosis of copper-related disorders to alleviate the risk of severe hepatic and neurological damage.[79,80] Further research is required to investigate the specific binding affinity of S_HICA with Cu^{2+} compared with other metal ions. In addition, finding a way to control the adsorption and desorption of Cu^{2+} by S_HICA will expand its utility across various biomedical fields and ultimately benefit the healthcare and pharmaceutical industries.

4. Experimental Section

Materials: Citric acid, histidine, dimethyl sulfoxide (DMSO), 3-(4,5-dimethylthiazol-2-yl)-2,5-diphenyltetrazolium bromide (MTT), fluorescein-5-isothiocyanate (FITC) and metal ions with chloride form including Fe^{3+}, Gd^{3+}, Al^{3+}, Mg^{2+}, Cu^{2+}, Cd^{2+}, K^{+}, and Cs^{+} were purchased from Sigma–Aldrich (St. Louis, Mo, USA.). Dialysis membranes (molecular weight cut off, 100–500 Da) were purchased from Spectrum Laboratories (Rancho Dominguez, CA, USA). Dulbecco's modified Eagle's medium (DMEM), Fetal bovine serum (FBS), and Dulbecco's phosphate-buffered saline (DPBS) were purchased from Hyclone Laboratories (Logan, UT, USA) analytical grade.

Synthesis of Carbon Dots: Carbon dots were prepared by using citric acid and histidine as the precursors and microwave synthesizer were used using Discover 2.0 (CEM, NC, USA). Distilled water and DMSO were employed as the solvents for HICA and S_HICA, respectively. Briefly, 250 mg of citric acid monohydrate and 549 mg of histidine were added to 10 mL of distilled water for HICA and to 10 mL of DMSO for S_HICA. Each solution was placed in a 35-mL vial and pre-stirred for 3 min. The vial was then placed in a reactor, and the solution was stirred for 5 min at 300 W and 220 °C. The solution was then diluted with distilled water and subjected to the first filtration by a syringe filter unit (PTFE, 0.45 µm, 25 mm, ADVANTEC). The solution was then dialyzed for 3 days by using a dialysis bag with a molecular weight cutoff range of 100–500 Da to remove the precipitant and unreacted precursors. The solution underwent another filtration process by a syringe filter unit (CA, 0.45 µm, 25 mm, ADVANTEC), after which it was freeze dried for 5 days.

Characterization of Carbon Dots: Dynamic light scattering (DLS), transmission electron microscopy (TEM), X-ray diffractometer (Miniflex600, Rigaku, Japan), atomic force microscope (AFM), X-ray photoelectron spectroscope (XPS, AXOS-HIS, KRATOS, United Kingdom), fourier

transform infrared spectroscopy (cary 630, Agilent, USA) and Elemental analyzer (Flash2000, thermo, USA) were utilized to characterize carbon dots. DLS was measured on a zetasizer nano ZS (Malvern, USA) at 25 °C in water. To prepare the specimens for TEM, carbon dots were dispersed in distilled water, and 20 µl of carbon dots were dropped on the grid. The specimens were air-dried and TEM observation was performed using JEM-2100F (JEOL, Japan). XRD data of carbon dots was obtained with Cu X-ray tube and 40kV. The scan range was set from $2\theta = 3°$–$90°$ with $10° \text{ min}^{-1}$ as a scan speed. For the AFM (XE7, Park Systems, Suwon, South Korea), a microscope probe (PPP-NCHR, Park Systems, Suwon, South Korea) with a resonance frequency of 330 kHz and a spring constant of 42 N m^{-1} was selected as the cantilever.

Fluorescent Evaluation of Carbon Dots: A Spectro fluorophotometer (RF-5301PC, Shimadzu) was utilized for excitation-emission intensity spectra and fluorescence stability analysis. For the excitation-emission intensity spectra, carbon dots were dissolved in distilled water. The fluorescence stability of the carbon dots (S_HICA and HICA) and FITC were evaluated for a range of environmental conditions. Specific excitation and emission wavelengths assigned to different samples: 470 and 540 nm, respectively, for S_HICA; 340 and 410 nm, respectively, for HICA, and 495 and 519 nm, respectively, for FITC.[81] And the fluorescence intensity of the carbon dots and FITC was measured at multiple time points for 3 days at interval of 12 h across varying pH levels from 1 to 11. For the fluorescence images of HICA and S_HICA were analyzed using Fluorescence-labeled Organism BioImaging (FOBI, NEO science, Korea).

Fluorescence Stability of the Carbon Dots and FITC: To acquire the cell pellet images of L929 cells incubated with carbon dot, the cells were seeded in a 100 mm cell culture dish at a density of 2.2×10^6 cells per dish and cultured for 2 days. Following the incubation, the cells were treated with various concentrations (1, 5, and 10 mg mL^{-1}) of carbon dots for 4 h. After the treatment, the cells were washed with DPBS and harvested using trypsin. Then, the harvested cells were centrifuged at 1500 rpm for 3 min and resulting cell pellet images were obtained using FOBI.

Evaluation of Metal Ions Detection: For the evaluating the metal ion detection capabilities of S_HICA, 1 mL of S_HICA aqueous solutions (0.1, 0.5, and 1 mg mL^{-1}) were prepared and mixed with 1 mL of various metal ions with concentrations ranging from 0 to 500 µM. The fluorescence spectra of the mixtures were observed through spectrofluorophotometer, utilizing excitation wavelengths ranging from 300 to 600 nm and emission wavelengths from 300 to 700 nm. The ratio of fluorescence intensity with and without metal ions, using an excitation wavelength of 470 nm, was measured to investigate the selectivity of S_HICA toward various metal ions.[82] The limit of detection (LOD) of the S_HICA toward Cu^{2+} was determined using the standard deviation of the blank(σ) and the slope of the calibration curve. The LOD was calculated using the following equation:

$$LOD = \frac{3 \times \sigma}{\text{Slope of calibration curve}} = 5.41\,\mu\text{M} \quad (1)$$

Quenching Mechanism Analysis: In presence of Cu^{2+} quenching mechanism of S_HICA was evaluated by cryo-TEM imaging and UV–vis spectra. S_HICA solution (10 mg mL^{-1}) was mixed with Cu^{2+} solution (1mM) and incubated for 30 min to fabricate S_HICA/Cu^{2+} complex due to the quenching effect. Subsequently, the mixture was heated to 80 °C for 10 min using a dry bath (Corning, USA). Each mixture, with and without heating, was vortexed prior to preparing cryogenic samples and each solution was mounted on glow discharged lacey carbon grid (Lacey Carbon, 200 mesh Cu, Ted Pella Inc., USA), respectively. Sample vitrification was performed using a Vitrobot Mark IV (Thermo Fisher Scientific, SNU CMCI), maintaining the chamber at 15 °C and 100% humidity. After mounting the solution, the excess solution was blotted away and immediately plunged into liquid ethane for freezing and stored in liquid nitrogen before cryo-TEM imaging. The cryogenic samples were loaded to a cryo-TEM holder (626 single tilt cryo-TEM holder, Gatan, USA), which maintained the temperature of the sample at ≈−180 °C. The cryo-TEM holder was loaded into a TEM, and images were acquired at an accelerating voltage of 200 kV. In addition, UV–vis spectra of S_HICA/Cu^{2+} complex were examined depending on the temperature. S_HICA/Cu^{2+} complex was prepared by mixing S_HICA solution (10 mg mL^{-1}) with Cu^{2+} solution (1mM) followed by incubation for 30 min. UV–vis absorption was measured while gradually increasing the temperature to 80 °C at a rate of 10 °C min^{-1}. In addition, chemical structural properties of the S_HICA/Cu^{2+} complex was evaluated using Selected Area Electron Diffraction (SAED) analysis after mounting the sample solution on the lacey carbon grid. Furthermore, to investigate the effect of the temperature on the fluorescence intensity of S_HICA/Cu^{2+} complex, fluorescence spectra were recorded at various temperatures ranging from 25 to 80 °C using an RF-6000 fluorescence spectrophotometer (Shimadzu, Japan). The excitation wavelength was set at 470 and fluorescence emission was recorded at 540 nm. The samples were incubated at each temperature for 5 min before measurements.

Fluorescence Lifetime Analysis: Fluorescence lifetime measurements were conducted at the Research Institute of Advanced Materials (RIAM), Seoul National University, using a FluoTime 300 (Picoquant, Germany). The excitation wavelength was set at λ_ex = 405 nm. For the measurements, 5 mg mL^{-1} of S_HICA mixed with various concentrations of Cu^{2+} and analyzed to investigate fluorescence quenching behavior. The fluorescence decay curve was fitted using Fluofit software to extract lifetime parameters.

Cell culture and Incubation Conditions: L929 cells (i.e., normal cell line of mouse connective tissue) were sourced from the Korean Cell Line Bank (KCLB) with the assigned number 10 001. The L929 cells were cultured in Dulbecco's modified Eagle medium (DMEM) supplemented with 10% fetal bovine serum (FBS) and 1% penicillin–streptomycin. The cells were incubated at 37 °C in 5% CO_2 with the culture medium being refreshed every 2–3 days.

Cytotoxicity Assay: The cytotoxic effects of S_HICA, HICA, and Cu^{2+} were evaluated by using the 3-(4,5-dimethylthiazol-2-yl)-2,5-diphenyltetrazolium bromide (MTT) assay on L929 cells as described in a previous study.[83] The L929 cells were cultured in 48 well plates at a concentration of 2×10^4 cells per well, which was followed by 24 h of incubation. Subsequently, the cells were exposed to varying concentrations of S_HICA, HICA, and Cu^{2+} for 4 h. The plates were then washed twice with DPBS, and MTT reagents were added for an additional 4 h of treatment. Formazan crystals were then dissolved in DMSO, and the absorbance at 450 nm was detected by using a microplate reader (Synergy H1, BioTeK, USA). The samples were dissolved in serum-free (SF) medium.

Flow Cytometry: To investigate the applicability of S_HICA as a phosphor for cell fluorescence imaging, L929 cells were seeded in six well plates at a cell density of 3×10^5 cells per well and were cultured for 24 h following a similar procedure as described in a previous study.[84] The cells were subsequently incubated with varying concentrations of S_HICA for various incubation times. The cells were then harvested and resuspended in DPBS. The fluorescence intensity of S_HICA within the cells was measured by a flow cytometer (Becton-Dickinson FACS Canto II).

Confocal Laser Scanning Microscopy: To visualize the interaction between S_HICA and Cu^{2+} in a cellular environment, L929 cells were seeded in six well plates with coverslips at a density of 3×10^5 cells per well and were cultured for 24 h. The cells were then exposed to Cu^{2+} at various concentrations of 0–100 µM for 4 h, which was followed by washing with DPBS and treatment with 0.1 mg mL^{-1} S_HICA for another 4 h. Afterward, the cells were fixed in 4% paraformaldehyde at 25 °C, and the fluorescence was imaged by using a confocal laser scanning microscope. The images were analyzed by using the software LSM Image Browser.

Ex vivo and in vivo Animal Experiment: The animal experiments adhered to the guidelines for the care and use of laboratory animals set forth by the National Institutes of Health, USA (NIH Publication No. 85-23, revised 1996) and were approved by the Institutional Animal Care and Use Committee of The Catholic University of Korea (Approval number: CUK-IACUC-2021-020-02). The blood samples were collected from the cheek vein of the Balb/c male mouse and subjected to analysis. Following the isolation of serum from the blood, fluorescence measurements were conducted by introducing S_HICA and Cu^{2+} with an excitation wavelength of 470 nm and an emission wavelength of 540 nm. To evaluate the in vivo

Cu^{2+} detection ability of S_HICA, fluorescence imaging experiments were conducted using three-week-old Balb/c nude mice. S_HICA (50 µL, 0.5 mg mL^{-1}) was subcutaneously injected into the back of mice, and fluorescence imaging was conducted immediately using a FOBI. To assess the fluorescence quenching effect in the presence of Cu^{2+}, an additional injection of either free Cu^{2+} (50 µL, 200 µM), or a pre-mixed Cu^{2+}/EDTA solution (50 µL, 200 µM) was administrated at the same injection site. Following the administration, fluorescence imaging was performed again under the same conditions using FOBI. The fluorescence intensity was quantified and analyzed using FOBI software.

Statistical Analysis: Statistical analysis in relative fluorescent of S_HICA in presence of various metal ions and concentrations was assessed using a two-way ANOVA with Tukey. Statistical analysis in Fluorescence images of mice injected with S_HICA before and after the administration of Cu^{2+} was assessed using a two-way ANOVA with Sidak's multiple comparisons test. Significance levels were denoted as follows: $*p < 0.05$, $**p < 0.01$, $***p < 0.001$. All statistical analysis were performed using Prism 8 (GraphPad Software Inc.).

Supporting Information

Supporting Information is available from the Wiley Online Library or from the author.

Acknowledgements

This work was supported by the Basic Science Research Program (RS-2022-NR068971) of the National Research Foundation of Korea funded by the Ministry of Science and ICT (MSIT); and the National Research Foundation of Korea (NRF) grant funded by the Korean government (MSIT) (No. RS-2024-00405381, No. RS-2025-00513935, No. RS-2025-00521275, No. NRF-2021M3A9I4022936); and Korean Fund for Regenerative Medicine (KFRM) grant funded by the Korean government (the Ministry of Science and ICT, the Ministry of Health & Welfare, KFRM 24A0105L1).

Conflict of Interest

The authors declare no conflict of interest.

Data Availability Statement

The data that support the findings of this study are available from the corresponding author upon reasonable request.

Keywords

carbon dot, copper ion sensing, copper related disease diagnosis, fluorescence probes, fluorescence quenching

Received: November 12, 2024
Revised: February 10, 2025
Published online:

[1] S. Chatterjee, X. S. Li, F. Liang, Y. W. Yang, *Small* **2019**, *15*, 1904569.
[2] M. Moustakas, *Materials* **2021**, *14*, 549.
[3] X. Zheng, W. Cheng, C. Ji, J. Zhang, M. Yin, *Rev. Anal. Chem.* **2020**, *39*, 231.
[4] A. Depauw, E. Dossi, N. Kumar, C. Fiorini-Debuisschert, G. Huberfeld, M. H. Ha-Thi, N. Rouach, I. Leray, *Chem.–A Eur. J.* **2016**, *22*, 14902.
[5] D.-Y. Kim, S. Shinde, G. Ghodake, *Sci. Rep.* **2017**, *7*, 3966.
[6] T. Egawa, K. Hirabayashi, Y. Koide, C. Kobayashi, N. Takahashi, T. Mineno, T. Terai, T. Ueno, T. Komatsu, Y. Ikegaya, *Angew. Chem.* **2013**, *125*, 3966.
[7] C. Wang, H. Shi, M. Yang, Y. Yan, E. Liu, Z. Ji, J. Fan, *Mater. Res. Bull.* **2020**, *124*, 110730.
[8] M. S. Salman, M. N. Hasan, M. M. Hasan, K. T. Kubra, M. C. Sheikh, A. I. Rehan, R. Waliullah, A. I. Rasee, M. E. Awual, M. S. Hossain, *J. Mol. Struct.* **2023**, *1282*, 135259.
[9] B.-E. Kim, T. Nevitt, D. J. Thiele, *Nat. Chem. Biol.* **2008**, *4*, 176.
[10] Z. Tümer, L. B. Møller, *Eur. J. Human Genetics* **2010**, *18*, 511.
[11] S. Youl, K. Hee, J. Ah, S. Young, C. Kim, *Tetrahedron* **2016**, *72*, 5563.
[12] L. Chen, J. Min, F. Wang, *Signal Transduction Targeted Ther.* **2022**, *7*, 378.
[13] Y. Li, Y. Dong, X. Zhou, K. Fan, *MedComm—Biomater. Appl.* **2023**, *2*, e36.
[14] M. L. Turski, D. J. Thiele, *J. Biol. Chem.* **2009**, *284*, 717.
[15] Y. Chen, M. Wei, J. Lee, J. Zhao, P. Lin, Q. Wang, F. Li, D. Ling, *Adv. NanoBiomed. Res.* **2021**, *1*, 2100007.
[16] A. D. Chapp, S. Schum, J. E. Behnke, T. Hahka, M. J. Huber, E. Jiang, R. A. Larson, Z. Shan, Q. H. Chen, *Physiol. reports* **2018**, *6*, e13666.
[17] C. D. Quarles Jr, M. Macke, B. Michalke, H. Zischka, U. Karst, P. Sullivan, M. P. Field, *Metallomics* **2020**, *12*, 1348.
[18] S. Krishnan, *Sensors and Actuators Rep.* **2022**, *4*, 100078.
[19] J. A. Cotruvo Jr, A. T. Aron, K. M. Ramos-Torres, C. J. Chang, *Chem. Soc. Rev.* **2015**, *44*, 4400.
[20] J. Wang, J. Pei, G. Li, *Spectrochim. Acta, Part A* **2023**, *290*, 122287.
[21] S. Wang, J. Yu, P. Zhao, J. Li, S. Han, *J. Alloys Compd.* **2021**, *854*, 157195.
[22] X.-L. Yang, C. Ding, R.-F. Guan, W.-H. Zhang, Y. Feng, M.-H. Xie, *J. Hazard. Mater.* **2021**, *403*, 123698.
[23] J. Wang, H. Chen, F. Ru, Z. Zhang, X. Mao, D. Shan, J. Chen, X. Lu, *Chem.–A Eur. J.* **2018**, *24*, 3499.
[24] J. Chen, H. Chen, T. Wang, J. Li, J. Wang, X. Lu, *Anal. Chem.* **2019**, *91*, 4331.
[25] T. Wu, X.-j. Gao, F. Ge, H.-g. Zheng, *CrystEngComm* **2022**, *24*, 7881.
[26] S.-W. Lv, J.-M. Liu, C.-Y. Li, N. Zhao, Z.-H. Wang, S. Wang, *Chem. Eng. J.* **2019**, *375*, 122111.
[27] C. S. Muñiz, J. M. M. Gayón, J. I. G. Alonso, A. Sanz-Medel, *J. Anal. At. Spectrom.* **2001**, *16*, 587.
[28] K. Inagaki, N. Mikuriya, S. Morita, H. Haraguchi, Y. Nakahara, M. Hattori, T. Kinosita, H. Saito, *Analyst* **2000**, *125*, 197.
[29] V. Lopez-Avila, O. Sharpe, W. H. Robinson, *Anal. Bioanal. Chem.* **2006**, *386*, 180.
[30] R. Lamba, Y. Yukta, J. Mondal, R. Kumar, B. Pani, B. Singh, *ACS Appl. Bio Mater.* **2024**, *7*, 2086.
[31] D. K. Kar, V. Praveenkumar, S. Si, H. Panigrahi, S. Mishra, *ACS Omega* **2024**, *9*, 11050.
[32] H. Kim, K. S. Kim, K. Na, *J. Ophthal. Clinics and Res.* **2023**, *361*, 373.
[33] R. Cheng, Y. Xiang, R. Guo, L. Li, G. Zou, C. Fu, H. Hou, X. Ji, *Small* **2021**, *17*, 2102091.
[34] Y. Jeong, M. Jin, K. S. Kim, K. Na, *Biomater. Res.* **2022**, *26*, 27.
[35] W. Jiang, Y. Zhao, X. Zhu, H. Liu, B. Sun, *Adv. NanoBiomed. Res.* **2021**, *1*, 2000042.
[36] J. Dong, B. Li, J. Xiao, G. Liu, V. Baulin, Y. Feng, D. Jia, A. Y. Tsivadze, Y. Zhou, *Carbon* **2022**, *199*, 151.
[37] H. Shabbir, E. Csapó, M. Wojnicki, *Inorganics* **2023**, *11*, 262.
[38] L. Sun, Y. Liu, Y. Wang, J. Xu, Z. Xiong, X. Zhao, Y. Xia, *Opt. Mater.* **2021**, *112*, 110787.
[39] S. Ross, R.-S. Wu, S.-C. Wei, G. M. Ross, H.-T. Chang, *J. Food and Drug Anal.* **2020**, *28*, 677.

[40] H. Lu, C. Li, H. Wang, X. Wang, S. Xu, *ACS Omega* **2019**, *4*, 21500.
[41] S. Anwar, H. Ding, M. Xu, X. Hu, Z. Li, J. Wang, L. Liu, L. Jiang, D. Wang, C. Dong, *ACS Appl. Bio Mater.* **2019**, *2*, 2317.
[42] F. Yan, Z. Sun, H. Zhang, X. Sun, Y. Jiang, Z. Bai, *Microchim. Acta* **2019**, *186*, 1.
[43] N. Ahmed, M. Hussain, T. H. Qamar, S. ul Hassan, P. Xia, L. Ma, X. Gao, L. Deng, *Org. Electron.* **2025**, *139*, 107197.
[44] J. Mondal, R. Lamba, Y. Yukta, R. Yadav, R. Kumar, B. Pani, B. Singh, *J. Mater. Chem. C* **2024**, *12*, 10330.
[45] P. A. Rasheed, M. Ankitha, V. K. Pillai, S. Alwarappan, *RSC Adv.* **2024**, *14*, 16001.
[46] Q. Zhou, M. Shi, M. Wu, N. Zhao, P. Shi, Y. Zhu, A. Wang, C. Ye, C.-T. Lin, L. Fu, *Catalysts* **2023**, *14*, 8.
[47] Y. Sun, M. Wei, R. Liu, H. Wang, H. Li, Q. Kang, D. Shen, *Talanta* **2019**, *194*, 452.
[48] S. Venkatesan, A. J. Mariadoss, K. Arunkumar, A. Muthupandian, *Sens. Actuators, B* **2019**, *282*, 972.
[49] J. B. Essner, C. H. Laber, S. Ravula, L. Polo-Parada, G. A. Baker, *Green Chem.* **2016**, *18*, 243.
[50] J. Wei, X. Zhang, Y. Sheng, J. Shen, P. Huang, S. Guo, J. Pan, B. Feng, *Mater. Lett.* **2014**, *123*, 107.
[51] Q. Zhang, R. Wang, B. Feng, X. Zhong, K. Ostrikov, *Nat. Commun.* **2021**, *12*, 6856.
[52] C. Li, J. Huang, L. Yuan, W. Xie, Y. Ying, C. Li, Y. Yu, Y. Pan, W. Qu, H. Hao, *Theranostics* **2023**, *13*, 3064.
[53] I. Karbhal, A. Basu, A. Patrike, M. V. Shelke, *Carbon* **2021**, *171*, 750.
[54] B. Geng, J. Hu, Y. Li, S. Feng, D. Pan, L. Feng, L. Shen, *Nat. Commun.* **2022**, *13*, 5735.
[55] G. Jeong, J. M. Lee, J. ah Lee, J. Praneerad, C. A. Choi, P. Supchocksoonthorn, A. K. Roy, W.-S. Chae, P. Paoprasert, M. K. Yeo, *Appl. Surf. Sci.* **2021**, *542*, 148471.
[56] A. Iqbal, F. B. Shittu, M. N. M. Ibrahim, N. A. Bakar, N. Yahaya, K. Rajappan, M. H. Hussin, W. H. Danial, L. D. Wilson, *Catalysts* **2022**, *12*, 1311.
[57] S. Deng, E. Zhang, Y. Zhao, H. Guo, L. Luo, S. Yi, B. Zheng, X. Mu, K. Yuan, X. Deng, *Comp. Biochem. Physiol. Part C: Toxicol. Pharmacol.* **2024**, *279*, 109865.
[58] H. Ferjani, S. Abdalla, O. A. Oyewo, D. C. Onwudiwe, *Inorg. Chem. Commun.* **2024**, *160*, 111866.
[59] L. Wang, W. Li, L. Yin, Y. Liu, H. Guo, J. Lai, Y. Han, G. Li, M. Li, J. Zhang, *Sci. Adv.* **2020**, *6*, eabb6772.
[60] Y. Park, H. Jeong, Y. Seo, W. Choi, Y. Hong, *Sci. Rep* **2017**, *7*, 1.
[61] U. Baruah, N. Gogoi, A. Konwar, M. Jyoti Deka, D. Chowdhury, G. Majumdar, *J. Nanopart.* **2014**, *2014*, 178518.
[62] A. Kurdekar, L. A. A. Chunduri, E. P. Bulagonda, M. K. Haleyurgirisetty, V. Kamisetti, I. K. Hewlett, *Microfluid. Nanofluid.* **2016**, *20*, 1.
[63] X. Huang, W. Ye, J. Zhuang, C. Hu, H. Dong, B. Lei, Y. Liu, *ACS Sustainable Chem. Eng.* **2024**, *12*, 10399.
[64] X. Qie, M. Zan, P. Gui, *Front Bioeng. Biotechnol.* **2022**, *10*, 894100.
[65] R. Cai, L. Xiao, M. Liu, F. Du, Z. Wang, *Int. J. Nanomed.* **2021**, *2021*, 7195.
[66] Y. Shi, H. Xu, T. Yuan, T. Meng, H. Wu, J. Chang, H. Wang, X. Song, Y. Li, X. Li, *Aggregate* **2022**, *3*, e108.
[67] M. Jeesna, A. Nambiar, A. Sobha, *Materi. Today Commun.* **2023**, *37*, 107199.
[68] Q. Fu, N. Li, K. Lu, Z. Dong, Y. Yang, *Mater. Today Chem.* **2024**, *37*, 102032.
[69] G. Kalaiyarasan, J. Joseph, P. Kumar, *ACS Omega* **2020**, *5*, 22278.
[70] M. A. Issa, Z. Z. Abidin, S. Sobri, S. A. Rashid, M. A. Mahdi, N. A. Ibrahim, *Sci. Rep.* **2020**, *10*, 11710.
[71] K. Mahesh, S. Karpagam, *Sens. Actuators, B* **2017**, *251*, 9.
[72] A. Uslu, E. Özcan, S. O. Tümay, H. H. Kazan, S. Yeşilot, *J. Photochem. Photobiol. A: Chem.* **2020**, *392*, 112411.
[73] D. Y. Hur, E. J. Shin, *Bull. Korean Chem. Soc.* **2015**, *36*, 104.
[74] A. Kostryzhev, C. Slater, O. Marenych, C. Davis, *Sci. Rep.* **2016**, *6*, 35715.
[75] F. Noun, E. A. Jury, R. Naccache, *Sensors* **2021**, *21*, 1391.
[76] F. Zu, F. Yan, Z. Bai, J. Xu, Y. Wang, Y. Huang, X. Zhou, *Microchim. Acta* **2017**, *184*, 1899.
[77] X. Xue, H. Fang, H. Chen, C. Zhang, C. Zhu, Y. Bai, W. He, Z. Guo, *Dyes Pigm.* **2016**, *130*, 116.
[78] C. Ge, F. Pei, X. Wang, P. Zhang, H. Li, Z. Sai, Y. Yang, K. Chang, T. Ni, Z. Yang, *Bioorg. Chem.* **2025**, *154*, 108051.
[79] D. Tornabene, P. Bini, M. Gastaldi, E. Vegezzi, C. Asteggiano, E. Marchioni, L. Diamanti, *Neurol. Sci.* **2024**, *45*, 987.
[80] G. Crisponi, V. M. Nurchi, D. Fanni, C. Gerosa, S. Nemolato, G. Faa, *Coord. Chem. Rev.* **2010**, *254*, 876.
[81] W. Fawaz, J. Hasian, I. Alghoraibi, *Sci. Rep.* **2023**, *13*, 18641.
[82] R. Alexpandi, C. V. M. Gopi, R. Durgadevi, H.-J. Kim, S. K. Pandian, A. V. Ravi, *Sci. Rep.* **2020**, *10*, 12883.
[83] S. Lee, J. W. Kim, J. Park, H. K. Na, D. H. Kim, J. H. Noh, D. S. Ryu, J. M. Park, J.-H. Park, H.-Y. Jung, *ACS Appl. Mater. Interfaces* **2022**, *14*, 17621.
[84] J. Kim, W. Park, D. Kim, E. S. Lee, D. H. Lee, S. Jeong, J. M. Park, K. Na, *Adv. Funct. Mater.* **2019**, *29*, 1900084.